molecules

MDPI

Article

Cyclohexane Vibronic States: A Combined VUV Spectroscopy and Theoretical Study

Edvaldo Bandeira [1], Alessandra S. Barbosa [1], Nykola C. Jones [2], Søren V. Hoffmann [2], Márcio H. F. Bettega [1,*] and Paulo Limão-Vieira [1,3,*]

1 Departamento de Física, Universidade Federal do Paraná, Caixa Postal 19044, Curitiba 81531-980, PR, Brazil; bandeira@fisica.ufpr.br (E.B.); alessandra@fisica.ufpr.br (A.S.B.)
2 ISA, Department of Physics and Astronomy, Aarhus University, Ny Munkegade 120, DK-8000 Aarhus C, Denmark; nykj@phys.au.dk (N.C.J.); vronning@phys.au.dk (S.V.H.)
3 Atomic and Molecular Collisions Laboratory, Centre of Physics and Technological Research (CEFITEC), Department of Physics, NOVA School of Science and Technology, Universidade NOVA de Lisboa, 2829-516 Caparica, Portugal
* Correspondence: bettega@fisica.ufpr.br (M.H.F.B.); plimaovieira@fct.unl.pt (P.L.-V.); Tel.: +55-41-3361-3002 (M.H.F.B.); +351-21-294-78-59 (P.L.-V.)

Abstract: In this work, we provide results from a joint experimental and theoretical study of the vibronic features of cyclohexane (C_6H_{12}) in the photon energy range of 6.8–10.8 eV (182–115 nm). The high-resolution vacuum ultraviolet (VUV) photoabsorption measurements, together with quantum chemical calculations at the time-dependent density functional theory (TDDFT) level, have helped to assign the major electronic excitations to mixed valence–Rydberg and Rydberg transitions. The C_6H_{12} photoabsorption spectrum shows fine structure which has been assigned to CH_2 scissoring, $v'_3(a_{1g})$, CH_2 rocking, $v'_4(a_{1g})$, C–C stretching, $v'_5(a_{1g})$, and CCC bending/CC torsion, $v'_{24}(e_g)$, modes. Molecular structure calculations at the DFT level for the neutral and cationic electronic ground-states have shown the relevant structural changes that are operative in the higher-lying electronic states. Photolysis lifetimes in the Earth's atmosphere are shown to be irrelevant, while the main atmospheric sink mechanism is the reaction with the •OH radical. Potential energy curves have been obtained at the TDDFT level of theory, showing the relevance of interchange character mainly involving the CH_2 scissoring, $v'_3(a_{1g})$, and CH_2 rocking, $v'_4(a_{1g})$, modes, while Jahn–Teller distortion yields weak vibronic coupling involving the non-totally symmetric CCC bending/CC torsion, $v'_{24}(e_g)$, mode.

Keywords: cyclohexane; cross-sections; theoretical calculations; spectroscopy

Academic Editor: Riccardo Chelli

Received: 7 March 2025
Revised: 21 March 2025
Accepted: 24 March 2025
Published: 27 March 2025

Citation: Bandeira, E.; Barbosa, A.S.; Jones, N.C.; Hoffmann, S.V.; Bettega, M.H.F.; Limão-Vieira, P. Cyclohexane Vibronic States: A Combined VUV Spectroscopy and Theoretical Study. *Molecules* **2025**, *30*, 1493. https://doi.org/10.3390/molecules30071493

1. Introduction

Cyclohexane, C_6H_{12}, is a chemical compound produced from the hydrogenation of C_6H_6, and it has been used as a fuel constituent in the combustion process, hence playing a role in vehicle emissions [1–4]. C_6H_{12} is a non-polar solvent widely used as an intermediate in the polymer industry, giving rise to significant emissions to the environment, as well as pollution reported from spills of petroleum products and the use of solvents [4], just to mention a few. It also contributes to the lower atmosphere local chemistry, mainly through reactions with •OH radicals [2,5,6], and can undergo oxidation processes yielding alkoxy radicals [5,7–10], among others. The main atmospheric implications of C_6H_{12} are related to its ability to act as an •OH radical scavenger while reacting with other chemicals, e.g., Cl and O_3 [5], thus relevant for consideration in modeling the atmospheric concentrations of volatile organic compounds (VOCs) [1]. Cyclohexane has been widely investigated by the

international community regarding the identification of effective processes to remove it as a toxic pollutant. Recently, Dahiru et al. [4] reported the use of non-thermal plasmas for the reduction of cyclohexane at room temperature and under atmospheric pressure.

Over the last two decades, we have been interested in investigating the role of some VOCs when released in the Earth's atmosphere [11–16]. To accomplish this purpose, we have produced comprehensive descriptions of the electronic state spectroscopy of such chemical compounds by recording high resolution photoabsorption spectra in the vacuum ultraviolet energy region, viz. 115–330 nm, together with the help of quantum chemical calculations. From the absolute values of the cross-sections above 180 nm, photolysis rates have been estimated from sea level (0 km) up to the limit of the stratopause (50 km altitude) (see [17] and the references therein). This joint experimental and theoretical effort is now being employed for C_6H_{12} in the wavelength region investigated in this work, i.e., from 115 nm (10.8 eV) up to 182 nm (6.8 eV).

The assignment of different absorption features requires detailed and complementary information from other spectroscopic techniques, whenever available. We note previous work on electron impact ionization [18–20], photoelectron spectroscopy [21,22], photoionization [21,22], and Penning ionization [23]. Other examples include the VUV photoabsorption with no complete assignments in the energy region of 5.5–31.0 eV [21,24–27] and infrared and Raman spectroscopies [28–30]. Finally, the modeling of atmospheric concentrations and rates of reaction with $^{\bullet}$OH radicals have been reported [1,2,5].

Section 2 deals with the structure and properties of cyclohexane, while Section 3 comprises the results and discussion, with a detailed description of the major electronic transitions and the fine structure assignments. Section 4 is devoted to a brief description of the experimental and theoretical methods. We close in Section 5 with the major conclusions from the present joint investigation of the electronic state spectroscopy of C_6H_{12}.

2. Structure and Properties of Cyclohexane

The total energy values with zero-point correction computed at the DFT/CAMB3LYP/aug-cc-pVTZ level of theory for cyclohexane conformers in the neutral ground-state and in the cationic ground-state show the *chair* and *boat* conformers, respectively, to be the most stable at room temperature (Table S1 and Figures S1 and S2).

The calculated outermost electronic configuration of the $\widetilde{X}^1A_{1g}$ ground-state is $(3e_u)^4$ $(1a_{1u})^2$ $(4e_u)^4$ $(4a_{1g})^2$ $(4e_g)^4$. The dominant transitions in the absorption spectrum (Figures 1–4, Table 1 and Table S2) have been assigned to electronic (and vibrational) excitations (Tables 2–4) involving the (HOMO), $4e_g$, $\sigma_{CC/CH}$, the (HOMO-1), $4e_g$, $\sigma_{CC/CH}$, the (HOMO-2), $4a_{1g}$, σ_{CH}, and the (HOMO-6, HOMO-7), $3e_u$, σ_{CH}, to mixed valence–Rydberg and Rydberg character orbitals (Table 1). The fine structures in the photoabsorption energy region 6.8–10.8 eV are assigned to vibrational modes from Raman and infrared spectroscopies [28–30], together with the calculated harmonic frequencies for the neutral electronic ground-state (Table S3) and the cation electronic ground-state (Table S4). The main modes have been assigned in the neutral electronic ground-state to 0.182 eV (1465 cm^{-1}) for CH_2 scissoring, $v_3''(a_{1g})$, 0.144 eV (1157 cm^{-1}) for CH_2 rocking, $v_4''(a_{1g})$, 0.099 eV (802 cm^{-1}) for C–C stretching, $v_5''(a_{1g})$, and 0.053 eV (426 cm^{-1}) for CCC bending/CC torsion, $v_{24}''(e_g)$ [31].

Table 5 lists the tentative assignments of the different Rydberg series based on their quantum defects. These have been obtained based on the lowest ionization vertical energies (IE_v) available from the photoelectron spectroscopy experiments of Kovac and Klasinc [32] to be $(IE_3)_v$ = 10.98 $(4e_u)^{-1}$ and $(IE_5)_v$ = 13.03 eV $(3e_u)^{-1}$. Rydberg series converging to $(4e_g)^{-1}$, $(4a_{1g})^{-1}$ and $(4a_{1u})^{-1}$ are dipole-forbidden within the molecule's D_{3d} group symmetry and are not assigned.

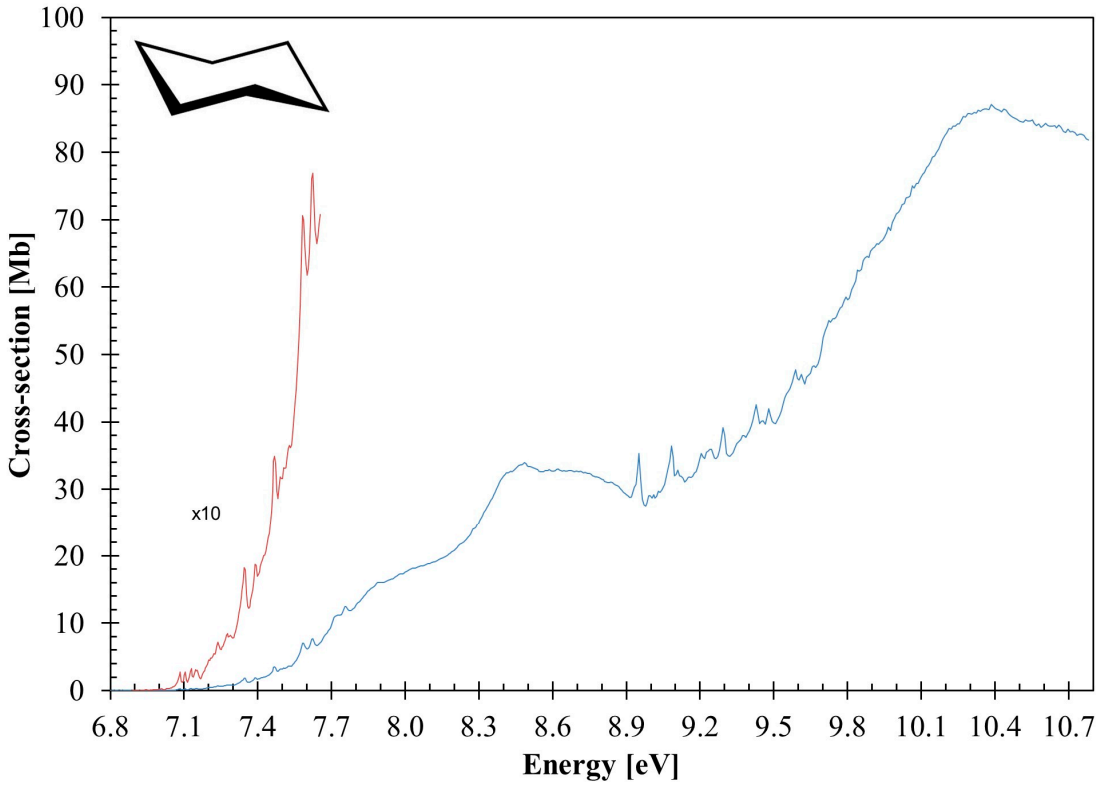

Figure 1. The photoabsorption spectrum of cyclohexane in the 6.8–10.8 eV photon energy range. See text for details.

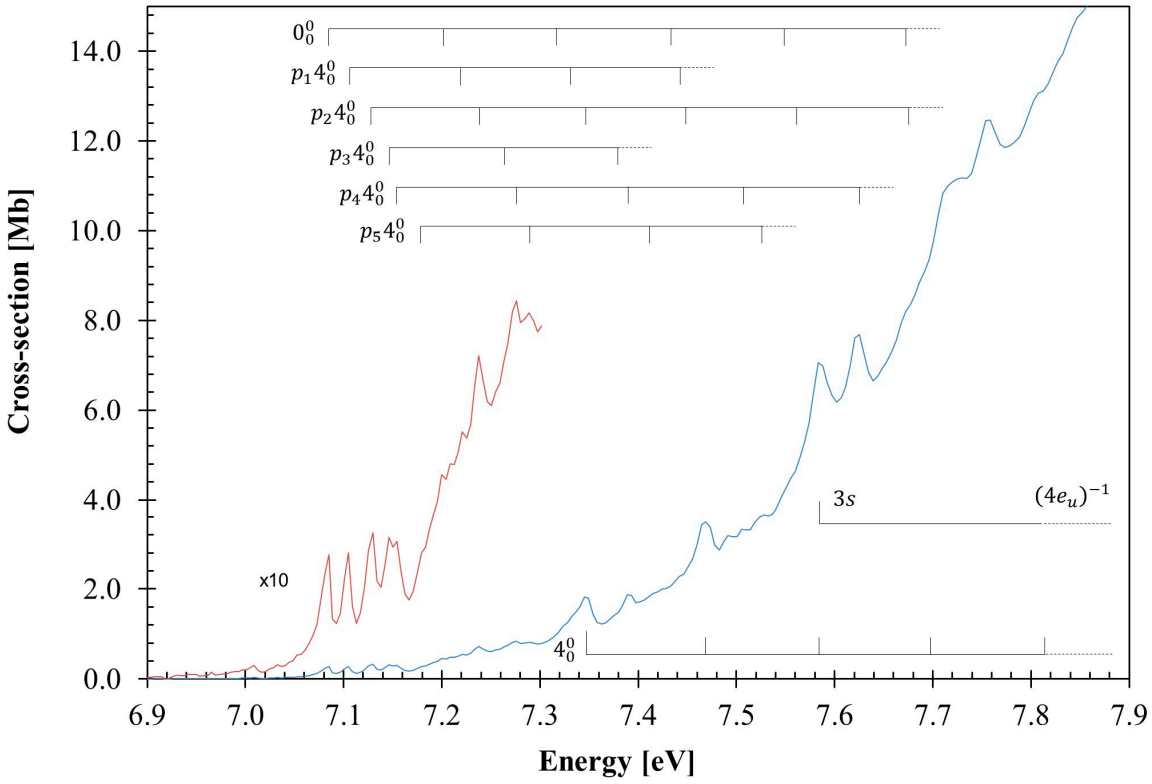

Figure 2. Detail of the photoabsorption spectrum of cyclohexane in the 6.9–7.9 eV photon energy range. See text for details.

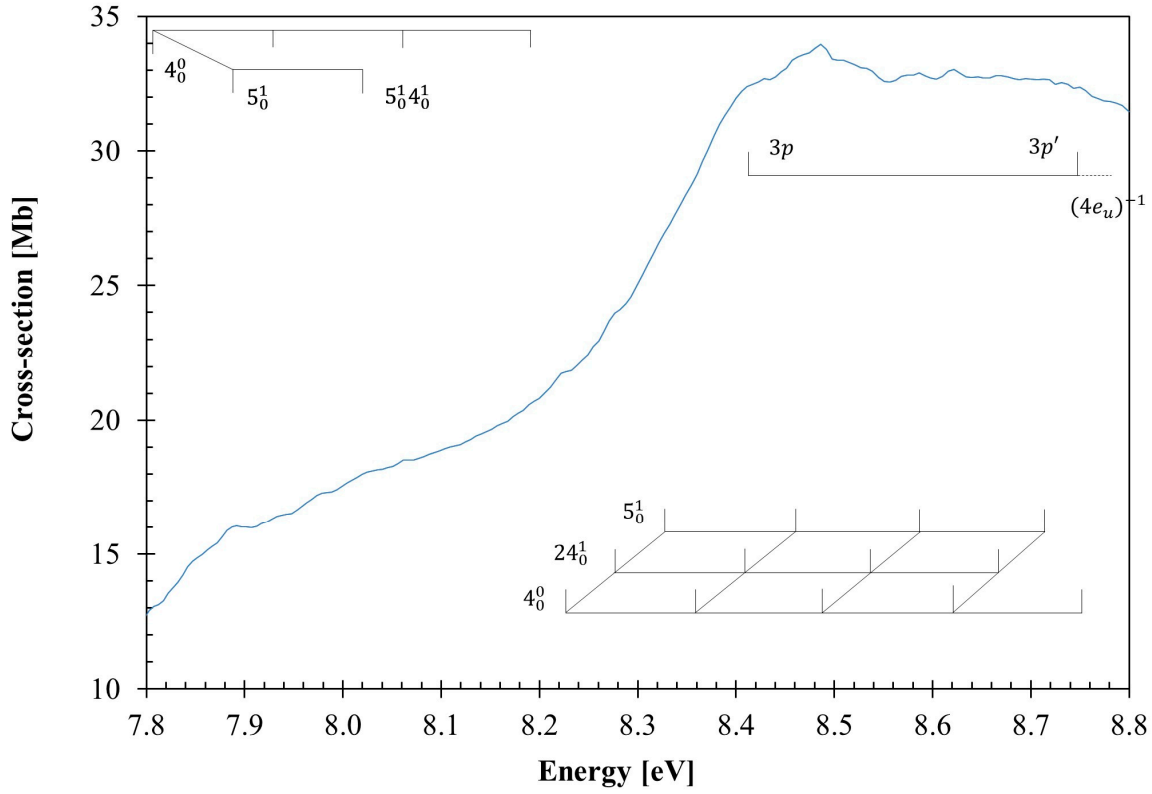

Figure 3. Photoabsorption spectrum of cyclohexane in the 7.8–8.8 eV photon energy range. See text for details.

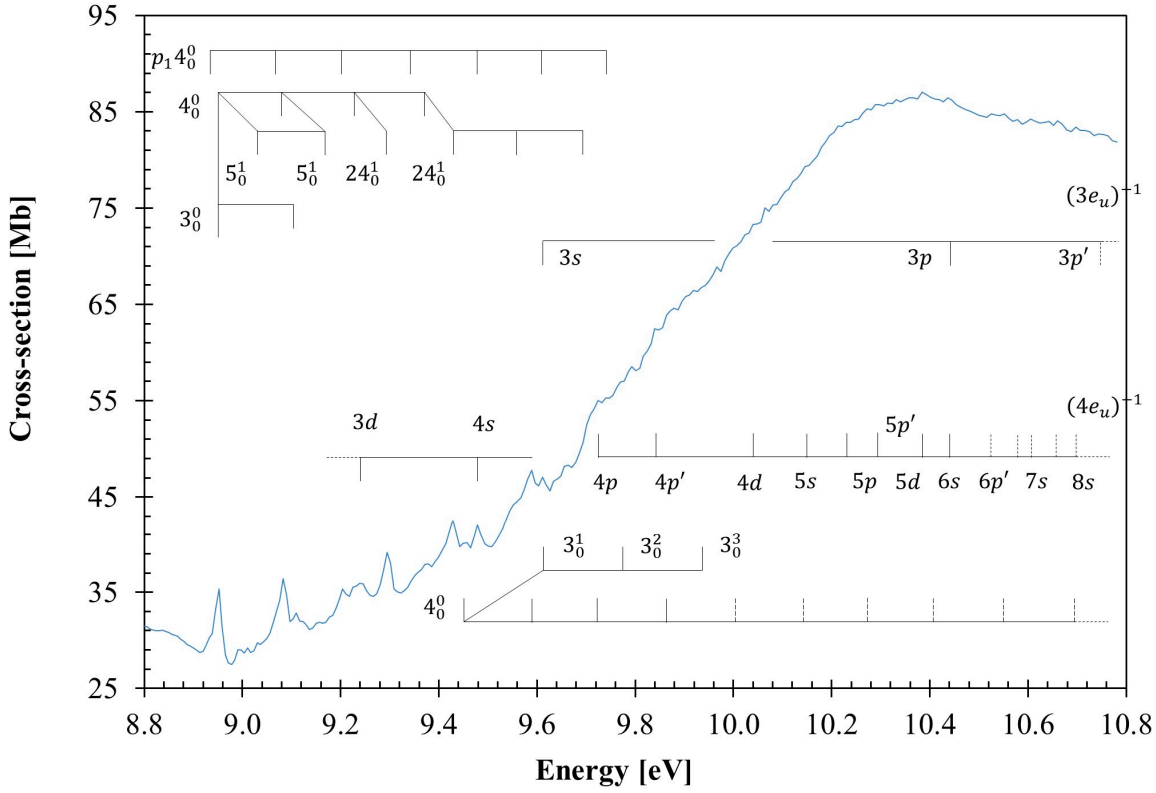

Figure 4. Photoabsorption spectrum of cyclohexane in the 8.8–10.8 eV photon energy range. See text for details. The vertical dashed lines show the tentative assignments of less-resolved features.

Table 1. The dominant calculated vertical excitation energies and oscillator strengths (TDDFT/CAMB3LYP/aug-cc-pVTZ) of cyclohexane compared with the present experimental data (energies in eV).

Cyclohexane					E (eV) Expt. [2]	Cross-Section (Mb)
State (D_{3d})	State (C_{2h})	E (eV)	f_L	Dominant Excitations [1]		
$\widetilde{X}^1A_{1g}$	$\widetilde{X}^1A_g$					
$1\,^1E_u$	$A_u \oplus B_u$	8.026	0.000172	$3p(4a_{2u}) \leftarrow \sigma_{CC/CH}(4e_g)$ (90%)	7.46(9)	3.49
$1\,^1A_{2u}$	B_u	8.147	0.002014	$3p'(5e_u) \leftarrow \sigma_{CC/CH}(4e_g)$ (44%), $3p''(5e_u) \leftarrow \sigma_{CC/CH}(4e_g)$ (44%)	8.02(0)	17.99
$2\,^1E_u$	$A_u \oplus B_u$	8.198	0.034207	$3p'(5e_u) \leftarrow \sigma_{CC/CH}(4e_g)$ (43%), $3p''(5e_u) \leftarrow \sigma_{CC/CH}(4e_g)$ (43%)	8.07(7)	18.57
$2\,^1A_{2u}$	B_u	8.487	0.221001	$3p(4a_{2u}) \leftarrow \sigma_{CH}(4a_{1g})$ (90%)	8.486	33.96
$5\,^1E_u$	$A_u \oplus B_u$	9.677	0.094079	$nf(5a_{2u}) \leftarrow \sigma_{CC/CH}(4e_g)$ (83%)	9.429	42.53
$8\,^1E_u$	$A_u \oplus B_u$	10.014	0.106166	$\sigma^*_{CH}/3s(5a_{1g}) \leftarrow \sigma_{CH}(3e_u)$ (28%), $nf(6a_{2u}) \leftarrow \sigma_{CC/CH}(4e_g)$ (33%), $\sigma^*_{CC}/ns(7a_{2u}) \leftarrow \sigma_{CC/CH}(4e_g)$ (13%)	9.92(7)	66.36
$10\,^1A_{2u}$	B_u	10.751	0.173676	$np(7a_{2u}) \leftarrow \sigma_{CH}(4a_{1g})$ (87%)	10.393	86.81

[1] We are not able to give the principal quantum number for the Rydberg members assigned with *n*. [2] The last decimal of the energy value is given in brackets for these less-resolved features.

Table 2. Proposed vibrational assignments of cyclohexane absorption bands in the photon energy range of 6.9−8.0 eV [a]; energies in eV.

Assignment	Energy	ΔE (ν_3')	ΔE (ν_4')	ΔE (ν_5')
$3p\ (4a_{2u}) \leftarrow \sigma_{CC/CH}(4e_g),\ \left(1^1E_u \leftarrow \widetilde{X}^1A_{1g}\right)$				
0_0^0	7.085	–	–	–
$p_1 4_0^0$	7.105	–	–	–
$p_2 4_0^0$	7.130	–	–	–
$p_3 4_0^0$	7.146	–	–	–
$p_4 4_0^0$	7.154	–	–	–
$p_5 4_0^0/5_0^1$	7.17(9) (s,w)	–	–	0.094
$4_0^1/p_1 5_0^1$	7.20(0) (s)	–	0.115	0.095
$p_1 4_0^1/p_2 4_0^0 5_0^1$	7.22(1) (w)	–	0.116	0.091
$p_2 4_0^1 3_0^1$	7.238	0.153	0.108	–
$p_3 4_0^1/p_4 5_0^1$	7.26(3) (s)	–	0.117	0.109
$p_4 4_0^1/p_2 3_0^1/p_5 4_0^0 5_0^1/5_0^2$	7.276	0.146	0.122	0.097
$p_5 4_0^1$	7.28(9) (w)	–	0.110	–
$4_0^2/p_2 4_0^0 5_0^2$	7.31(9) (s)	–	0.119	0.098
$p_1 4_0^2$	7.32(8) (s)	–	0.107	0.090
$p_2 4_0^2$	7.345	–	0.107	–
$p_3 4_0^2/p_4 4_0^1 5_0^1/p_2 3_0^1 5_0^1/p_5 4_0^0 5_0^2/5_0^3$	7.38(0) (s)	–	0.117	0.104
$p_4 4_0^2/p_2 3_0^2$	7.389	0.151	0.113	–
$p_5 4_0^2/4_0^2 5_0^1/p_2 4_0^0 5_0^3$	7.41(5) (s)	–	0.126	0.096
$p_4 4_0^1 3_0^1/p_2 3_0^2/p_5 4_0^0 5_0^1 3_0^1/5_0^2 3_0^1/p_1 4_0^2 5_0^1$	7.42(9) (s,w)	0.153	–	0.101
4_0^3	7.43(3) (s)	–	0.114	–
$p_1 4_0^3$	7.44(2) (s)	–	0.114	–
$p_2 4_0^3$	7.44(7) (s)	–	0.102	–
$p_4 4_0^3/p_2 3_0^2 4_0^1/p_5 4_0^2 5_0^1/4_0^2 5_0^2/p_2 4_0^0 5_0^4$	7.51(4) (s,b)	–	0.125	0.099
$p_5 4_0^3/p_4 4_0^1 3_0^1 5_0^1/p_2 3_0^2 5_0^1/p_5 4_0^0 5_0^2 3_0^1/5_0^3 3_0^1/p_1 4_0^2 5_0^2$	7.52(8) (b,w)	–	0.113	0.099
$4_0^4/p_4 4_0^2 3_0^1/p_2 3_0^3$	7.54(6) (s)	0.157	0.113	–
$p_2 4_0^4$	7.56(0) (s)	–	0.113	–
$p_4 4_0^1 3_0^2/p_2 3_0^3/p_5 4_0^0 5_0^1 3_0^2/5_0^2 3_0^2/p_1 4_0^2 5_0^1 3_0^1$	7.57(0) (s)	0.141	–	–
$p_4 4_0^4/p_2 3_0^2 4_0^2/p_5 4_0^3 5_0^1/p_4 4_0^1 3_0^1 5_0^2/p_2 3_0^2 5_0^2/p_5 4_0^0 5_0^3 3_0^1/5_0^4 3_0^1/p_1 4_0^2 5_0^3$	7.625	–	0.111	0.097
4_0^5	7.67(2) (s)	–	0.126	–
$p_2 4_0^5$	7.67(7) (s)	–	0.117	–
$4_0^4 3_0^1/p_4 4_0^2 3_0^2/p_2 3_0^4$	7.69(6) (s,b)	0.150	–	–
$4_0^4 3_0^2/p_4 4_0^2 3_0^3/p_2 3_0^5$	7.84(7) (s,w)	0.151	–	–
	$\overline{\Delta E}$	0.150	0.115	0.098
$3p/3p'\ (5e_u) \leftarrow \sigma_{CC/CH}(4e_g),\ \left(1^1A_{2u} \leftarrow \widetilde{X}^1A_{1g}\right)$				
0_0^0	7.345	–	–	–
4_0^1	7.46(9)	–	0.124	–

Table 2. *Cont.*

Assignment	Energy	ΔE (ν_3')	ΔE (ν_4')	ΔE (ν_5')
3_0^1	7.51(0) (w)	0.165	–	–
4_0^2	7.583	–	0.114	–
3_0^2	7.67(7) (s)	0.167	–	–
4_0^3	7.69(6) (s,b)	–	0.113	–
4_0^4	7.82(2) (s,b)	–	0.126	–
4_0^5	7.94(3) (s,b)	–	0.121	–
	$\overline{\Delta E}$	0.153	0.120	–

[a] (w) weak feature; (s) shoulder structure; (b) broad feature (the last decimal of the energy value is given in brackets for these less-resolved features).

Table 3. Proposed vibrational assignments of cyclohexane absorption bands in the photon energy range of 7.8−8.8 eV [a]; energies in eV.

Assignment	Energy	ΔE (ν_4')	ΔE (ν_5')	ΔE (ν_{24}')
$3p'/3p''\ (5e_u) \leftarrow \sigma_{CC/CH}(4e_g),\ \left(2^1E_u \leftarrow \widetilde{X}^1A_{1g}\right)$				
0_0^0	7.80(8) (s)	–	–	–
5_0^1	7.89(2) (s)	–	0.084	–
4_0^1	7.93(3) (s)	0.125	–	–
$5_0^1 4_0^1$	8.02(0) (s)	0.128	–	–
4_0^2	8.06(7) (s)	0.134	–	–
4_0^3	8.19(5) (s,w)	0.128	–	–
$3p\ (4a_{2u}) \leftarrow \sigma_{CH}(4a_{1g}),\ \left(2^1A_{2u} \leftarrow \widetilde{X}^1A_{1g}\right)$				
0_0^0	8.22(7) (s)	–	–	–
24_0^1	8.27(7) (s)	–	–	0.050
5_0^1	8.32(7) (s,w)	–	0.100	–
4_0^1	8.36(0) (s,w)	0.133	–	–
$4_0^1 5_0^1$	8.41(1) (s,b)	0.134	–	0.051
$4_0^1 24_0^1$	8.46(3) (s,w)	0.136	–	–
4_0^2	8.486	0.126	–	–
$4_0^2 5_0^1$	8.53(9) (s,w)	0.128	–	0.053
$4_0^2 24_0^1$	8.58(6) (w)	0.123	0.100	–
4_0^3	8.62(2) (b)	0.136	–	
$4_0^3 5_0^1$	8.67(0) (b,w)	0.131	–	0.048
$4_0^3 24_0^1$	8.71(9) (w)	0.133	0.097	–
4_0^4	8.75(0) (b,w)	0.128	–	–
	$\overline{\Delta E}$	0.130	0.095	0.051

[a] (s) shoulder structure; (w) weak feature; (b) broad feature (the last decimal of the energy value is given in brackets for these less-resolved features).

Table 4. Proposed vibrational assignments and progression of cyclohexane absorption bands in the photon energy range of 8.8−10.8 eV [a]; energies in eV.

Assignment	Energy	ΔE (ν_3')	ΔE (ν_4')	ΔE (ν_5')	ΔE (ν_{24}')
$nf\ (5a_{2u}) \leftarrow \sigma_{CC/CH}(4e_g),\ \left(5^1E_u \leftarrow \widetilde{X}^1A_{1g}\right)$					
$p_1 4_0^0$	8.93(3) (s)	–	–	–	–
0_0^0	8.952	–	–	–	–
5_0^1	9.03(7) (w)	–	–	0.084	–
$p_1 4_0^1$	9.06(3) (s)	–	0.130	–	–
4_0^1	9.083	–	0.131	–	–
3_0^1	9.110	0.158	–	–	–
$4_0^1 5_0^1$	9.17(0) (b)	–	0.133	0.087	–
$p_1 4_0^2$	9.205	–	0.142	–	–
4_0^2	9.23(2) (b)	–	0.149	–	–
$4_0^2 24_0^1$	9.294	–	0.124	–	0.062

Table 4. *Cont.*

Assignment	Energy	ΔE (ν_3')	ΔE (ν_4')	ΔE (ν_5')	ΔE (ν_{24}')
$p_1 4_0^3$	9.35(0) (s)	–	0.145	–	–
4_0^3	9.37(1) (w)	–	0.139	–	–
$4_0^3 24_0^1$	9.429	–	0.135	–	0.058
$p_1 4_0^4$	9.479	–	0.129	–	–
$4_0^4 24_0^1$	9.559	–	0.130	–	–
$p_1 4_0^5$	9.611	–	0.132	–	–
$4_0^5 24_0^1$	9.69(4) (s,w)	–	0.135	–	–
$p_1 4_0^6$	9.74(7) (w)	–	0.129	–	–
$\sigma_{CH}^*/3s\ (5a_{1g}) \leftarrow \sigma_{CH}(3e_u) + nf\ (6a_{2u})/\sigma_{CC}^*/ns\ (7a_{2u}) \leftarrow \sigma_{CC/CH}(4e_g)$, $\left(8^1E_u \leftarrow \widetilde{X}^1A_{1g}\right)$					
0_0^0	9.45(7) (w)	–	–	–	–
4_0^1	9.589	–	0.132	–	–
3_0^1	9.611	0.154	–	–	–
4_0^2	9.72(4) (w)	–	0.135	–	–
3_0^2	9.77(8) (s,b)	0.167	–	–	–
4_0^3	9.86(4) (s,w)	–	0.140	–	–
3_0^3	9.92(7) (s,w)	0.149	–	–	–
4_0^4	9.99(9) (s,w)	–	0.135	–	–
4_0^5	10.14(6) (s,w)	–	0.147	–	–
4_0^6	10.28(1) (s,w)	–	0.135	–	–
4_0^7	10.41(0) (s,w)	–	0.129	–	–
4_0^8	10.55(2) (s,w) *	–	0.142	–	–
4_0^9	10.69(8) (s,w) *	–	0.146	–	–
	$\overline{\Delta E}$	0.157	0.136	0.086	0.060

[a] (s) shoulder structure; (w) weak feature; (b) broad feature; * tentative assignment (the last decimal of the energy value is given in brackets for these less-resolved features).

Table 5. Energy values (eV), quantum defects (δ), and assignments of the Rydberg series converging to the $(4e_u)^{-1}\ \widetilde{B}^2E_u$ and $(3e_u)^{-1}\ \widetilde{D}^2E_u$ ionic electronic states of cyclohexane [a].

E_n	δ	Assignment	E_n	δ	Assignment
$(IE_3)_v$ = 10.98 eV $(4e_u)^{-1}$			**$(IE_5)_v$ = 13.03 eV $(3e_u)^{-1}$**		
$(ns \leftarrow 4e_u)$			$(ns \leftarrow 3e_u)$		
7.583	1.00	3s	9.611	1.00	3s
9.479	0.99	4s	–	–	–
10.14(6) (s,w)	0.96	5s	–	–	–
10.445	0.96	6s *	–	–	–
10.60(6) (w)	0.97	7s *	–	–	–
10.69(8) (w)	1.05	8s *	–	–	–
$(np \leftarrow 4e_u)$			$(np \leftarrow 3e_u)$		
8.41(1) (s,b)	0.70	3p	10.445	0.70	3p *
9.73(2) (s)	0.70	4p	–	–	–
10.23(4) (s,w)	0.73	5p	–	–	–
$(np' \leftarrow 4e_u)$			$(np' \leftarrow 3e_u)$		
8.75(0) (w)	0.53	3p′	10.76(3) (b,w)	0.55	3p′ *
9.84(8) (s)	0.53	4p′	–	–	–
10.29(8) (s,w)	0.53	5p′	–	–	–
10.52(5) (w)	0.53	6p′ *	–	–	–
10.66(1) (s,w)	0.47	7p′ *	–	–	–
$(nd \leftarrow 4e_u)$			$(nd \leftarrow 3e_u)$		
9.23(9) (b,w)	0.20	3d	–	–	–
10.03(9) (s)	0.20	4d	–	–	–
10.38(4) (w)	0.22	5d	–	–	–
10.57(9) (w)	0.17	6d *	–	–	–

[a] (s) shoulder structure; (w) weak feature; (b) broad structure; * tentative assignment (the last decimal of the energy value is given in brackets for these less-resolved features).

3. Discussion

The VUV photoabsorption spectrum of C_6H_{12} is shown in Figure 1 in the energy range 6.8 to 10.8 eV, while the fine structure and the Rydberg assignments are shown in the enlarged sections in Figures 2–4 (see also Tables 2–5). The major absorption bands have been assigned to electronic excitations from the ground-state to mixed valence–Rydberg and Rydberg molecular orbitals with the help of the TDDFT/CAMB3LYP/aug-cc-pVTZ calculations in Table 1. The results of the calculations also include the vertical excitation energies and oscillator strengths and are compared with the experimental data.

The Rydberg character is related to each series, converging to the different ionic electronic states $(4e_u)^{-1}\ \widetilde{B}^2E_u$ and $(3e_u)^{-1}\ \widetilde{D}^2E_u$ (see Section 3.4). At a glance, the absorption bands are rather broad, and the spectrum baseline is continuously shifted above the baseline as the photon energy increases. The dominant electronic excitations in Table 1 are Rydberg, and only mixed valence–Rydberg character is noted above 9.9 eV. However, a close inspection of the complete set of electronic transitions (Table S2) and the representation of cyclohexane molecular orbitals (Figure S3) show that while the character of the unoccupied molecular orbitals is mostly Rydberg, there are minor contributions from σ^*_{CC} and σ^*_{CH} antibonding MOs. Thus, the latter may render an underlying dissociative character of the electronic transitions to the photoabsorption cross-section.

The fine structure noted throughout the photoabsorption spectrum in the energy range of 6.8–10.8 eV (Figures 1–4) has been assigned to the contribution of the CH_2 scissoring, $v'_3(a_{1g})$, the CH_2 rocking, $v'_4(a_{1g})$, the C–C stretching, $v'_5(a_{1g})$, and the CCC bending/CC torsion, $v'_{24}(e_g)$, modes. A detailed assignment of this structure, associated with the electronic transitions from Table 1, are listed in Table 2.

The results from the calculations in Table 1 show a good level of agreement with the experimental data for all electronic transitions to within 3%; however, the major difference is noted for the lowest-lying electronic transition, where this value increases to ~7%. The calculations have been performed in the C_{2h} symmetry group and correlating with the D_{3d} point group as $A_u \oplus B_u \rightarrow E_u$ and $B_u \rightarrow A_{2u}$ for the dominant excitations. The next section contains a detailed description of the electronic (and vibrational) excitations, with the major transitions and their origins tentatively assigned, absolute cross-section values compared with others in the literature, and discussion about cyclohexane photolysis.

3.1. The 7.0–7.9 eV Photon Energy Range

The lowest-lying valence excitation is assigned to an electron promotion from the degenerate HOMO/HOMO-1, $4e_g$, $\sigma_{CC/CH}$ orbital to the LUMO+1 Rydberg molecular orbital (see Tables 1 and S2, and Section 3.4), $3p\ (4a_{2u}) \leftarrow \sigma_{CC/CH}(4e_g)$, $\left(1^1E_u \leftarrow \widetilde{X}^1A_{1g}\right)$, with a cross-section value of 3.49 Mb at 7.46(9) eV (Figure 2). The calculated vertical excitation energy of 8.026 eV and an oscillator strength $f_L \approx 0.00017$ are ~7% higher than the experimental value. The 0^0_0 origin is tentatively assigned at 7.085 eV, while the VUV spectrum of Raymonda [26] shows a feature at 7.005 eV (56,500 cm^{-1}), showing up to five progressions of the CH_2 rocking, $v'_4(a_{1g})$, mode, as listed in Table 2. Moreover, some of the features can be assigned to combinations of the CH_2 scissoring, $v'_3(a_{1g})$ mode, while the C–C stretching, $v'_5(a_{1g})$ mode can also contribute to the spectrum. To avoid the congestion of Figure 2, $v'_3(a_{1g})$ and $v'_5(a_{1g})$ were not included, but the different energy values can be obtained from Table 2. The average spacings of $v'_3(a_{1g})$, $v'_4(a_{1g})$, and $v'_5(a_{1g})$ are 0.150 eV (1210 cm^{-1}), 0.115 eV (936 cm^{-1}), and 0.098 eV (790 cm^{-1}), respectively. The feature at 7.583 eV is assigned to the first member of a Rydberg series converging to the $(4e_u)^{-1}\ \widetilde{B}^2E_u$ ionic electronic state, which will be discussed in Section 3.4.

The second absorption band tentatively centered at 8.02(0) eV, with a maximum cross-section of 17.99 Mb, is assigned to the Rydberg excitation (Section 3.4) $3p/3p'\ (5e_u) \leftarrow \sigma_{CC/CH}(4e_g)$,

$\left(1^1A_{2u} \leftarrow \widetilde{X}^1A_{1g}\right)$, with an oscillator strength of ≈0.00201 (Table 1). The 0_0^0 origin band is assigned at 7.345 eV (Table 2 and Figure 2) from its broadness related to a vibrational excitation, as well as from the shape of its left-hand side, showing a different slope from that of the former electronic state's features. This band shows broad features, which are due to CH_2 rocking, $v_4'(a_{1g})$ mode, and combinations with CH_2 scissoring, $v_3'(a_{1g})$ mode, with average spacings of 0.153 eV (1234 cm^{-1}) and 0.120 eV (968 cm^{-1}), respectively.

3.2. The 7.8–8.8 eV Photon Energy Range

The photoabsorption spectrum in this energy range includes two electronic transitions centered at 8.07(7) and 8.486 eV (Figure 3), which are assigned to Rydberg transitions, with cross-section values of 18.57 and 33.96 Mb (Table 1 and Figure 3). The 0_0^0 origin bands are assigned at 7.80(8) and 8.22(7) eV and are accompanied by excitation of CH_2 rocking, $v_4'(a_{1g})$, and C–C stretching, $v_5'(a_{1g})$ modes, and combinations with CCC bending/CC torsion, $v_{24}'(e_g)$ mode, with mean energy values of 0.130, 0.095 and 0.051 eV, respectively (Table 2). The Rydberg excitations are assigned to $3p(4e_u)^{-1}$ and $3p\prime(4e_u)^{-1}$ (see Section 3.4), although this is not in agreement with the character of the calculated electronic transition in Table 1, $3p\prime/3p\prime\prime\ (5e_u) \leftarrow \sigma_{CC/CH}(4e_g)$, $\left(2^1E_u \leftarrow \widetilde{X}^1A_{1g}\right)$, and $3p\ (4a_{2u}) \leftarrow \sigma_{CH}(4a_{1g})$, $\left(2^1A_{2u} \leftarrow \widetilde{X}^1A_{1g}\right)$.

3.3. The 8.8–10.8 eV Photon Energy Range

From the theoretical calculations in Table 1, the absorption features in this photon energy region are assigned as mixed valence–Rydberg and Rydberg in character, with vibrational fine structure. Figure 4 shows an expanded view of the photoabsorption spectrum, and the proposed assignments are summarized in Table 4. Most of the Rydberg features appear too broad rather than narrow, and are barely visible in the high energy region of the photoabsorption band. This is due to their energy positions being superimposed on the extensive vibrational progressions of other Rydberg series, spanning from 8.8 up to 10.8 eV, and to the relevant dissociative nature of the σ_{CH}^* antibonding valence state (see Table 1).

The three dominant electronic states peaking at 9.429, 9.92(7), and 10.393 eV, with cross-section values of 42.53, 66.36, and 86.81 Mb, and calculated oscillator strengths of ≈0.09408, ≈0.10617, and ≈0.17368, respectively, are assigned to $nf\ (5a_{2u}) \leftarrow \sigma_{CC/CH}(4e_g)$, $\left(5^1E_u \leftarrow \widetilde{X}^1A_{1g}\right)$, $\sigma_{CH}^*/3s\ (5a_{1g}) \leftarrow \sigma_{CH}(3e_u) + nf\ (6a_{2u})/\sigma_{CC}^*/ns\ (7a_{2u}) \leftarrow \sigma_{CC/CH}(4e_g)$, $\left(8^1E_u \leftarrow \widetilde{X}^1A_{1g}\right)$, and $np\ (7a_{2u}) \leftarrow \sigma_{CH}(4a_{1g})$, $\left(10^1A_{2u} \leftarrow \widetilde{X}^1A_{1g}\right)$ (see Table 1). The 0_0^0 transitions are tentatively assigned at 8.952, 9.45(7), and 9.73(2) eV, respectively, (Tables 4 and 5), and show a fine structure superimposed on the Rydberg series (see discussion in Section 3.4). Note that for the first transition, there is also a progression of the CH_2 rocking, $v_4'(a_{1g})$ mode, as listed in Table 4. The vertical dashed lines in Figure 4 show the tentative assignments of less-resolved features.

3.4. Rydberg Transitions

The photoabsorption spectrum above 7.5 eV shows features that have been assigned to different Rydberg transitions, with fine structure in some of the measured photon energy regions (Figures 2–4). These Rydberg states converge to $(4e_u)^{-1}\ \widetilde{B}^2E_u$ and $(3e_u)^{-1}\ \widetilde{D}^2E_u$ ionic electronic states of cyclohexane and have been assigned in Table 5, according to their positions and the quantum defects obtained from the Rydberg formula: $E_n = IE - R/(n-\delta)^2$, where IE is ionization energy of a given MO, n is the principal quantum number of the Rydberg orbital of energy E_n, R is the Rydberg constant (13.61 eV), and δ is the quantum defect resulting from the penetration of the Rydberg orbital into the core.

A higher uncertainty of features in the spectrum due to increased noise at the highest energies means that only tentative assignments are made above 10.4 eV and are marked as dashed lines in Figure 4. Nonetheless, the lowest-lying Rydberg transition (n = 3) converging to the ionic electronic second excited state IE_3, $(4e_u)^{-1}$, is assigned to the $(3s \leftarrow 4e_u)$ excitation, with the first member at 7.583 eV and a quantum defect δ = 1.00. Higher-order Rydberg members of the ns series up to n = 8 are reported in Table 5. The first members of the two $(np \leftarrow 4e_u)$ and $(np\prime \leftarrow 4e_u)$ series display absorption features at 8.41(1) eV and 8.75(0) eV (δ = 0.70 and 0.53). In Table 5, we also include an nd $(nd \leftarrow 4e_u)$ series with principal quantum numbers up to n = 6, where n = 3 has been assigned at 9.23(9) eV (δ = 0.20). The features at 10.445 eV could also be assigned to $3p(3e_u)^{-1}$.

The Rydberg series converging to the ionic electronic fourth excited state IE_5, $(3e_u)^{-1}$, are listed in Table 5, and have been assigned to the $(ns,\ np, np\prime \leftarrow 3e_u)$ transitions. The members of these series are only n = 3, and are associated with features at 9.611, 10.445, and 10.76(3) eV, with quantum defects δ = 1.00, δ = 0.70, and δ = 0.55, respectively (Table 3). Higher members of these series lie outside the energy range investigated here.

To assess the role of different vibrational modes assigned in the absorption spectrum to the molecular structure of cyclohexane, we have obtained, at the DFT/CAMB3LYP/aug-cc-pVTZ level, the bond lengths in Å and bond angles in (°) for the neutral *chair* ground-state (Figure S1) and the cationic *boat* ground-state (Figure S2). A close comparison between the two molecular structures shows that upon ionization, minor changes up to 3% are noted within the bond lengths. However, relevant shortenings of 10 and 11% are observed within the H11–C3–C4 (also H15–C5–C4 and H17–C6–C1) and H9–C2–C1 angles. These changes are consistent with the general molecular deformation related to CH_2 rocking, $v'_4(a_{1g})$ and CCC bending/CC torsion $v'_{24}(e_g)$ modes. Another interesting aspect is related to a modest 7% decrease in ∠ C5–C4–C3, which may also render a contribution to CH_2 scissoring, $v'_3(a_{1g})$, and C–C stretching, $v'_5(a_{1g})$, modes, relevant in the vibrational excitation within the Rydberg transitions listed in Tables 3 and 4 (see also Figures 3 and 4).

3.5. Potential Energy Curves for CH_2 Scissoring and CH_2 Rocking Coordinates

We have obtained potential energy curves (PECs) for the ten lowest excited states of cyclohexane (Figure 5), following the normal coordinates associated with the vibrational modes CH_2 scissoring, $v'_3(a_{1g})$, and CH_2 rocking, $v'_4(a_{1g})$ (in a_0 units). Some of the electronic transitions are not allowed within the D_{3d} symmetry point group, i.e., f_L = 0 in Table S1. However, upon electronic excitation from the ground-state and within the normal coordinate displacement (Figure 5), symmetry is broken. Therefore, the calculations have been performed at the TDDFT/CAMB3LYP/aug-cc-pVTZ level of theory in the C_1 symmetry group, while allowing all atoms to relax following the respective mode.

A close inspection of Figure 5 shows that all states are bound within the reaction coordinates, which is in support of the fine structure involving these modes throughout the different sections of the photoabsorption spectrum. Additionally, the PECs show quasi-degenerate behavior and avoided crossings for most of the calculated electronic states. Thus, within the adiabatic description of the nuclear dynamics, as the normal coordinate is changed, an interchange between states may be possible, i.e., within Rydberg characters. Note that in case of C–C stretching $v'_5(a_{1g})$ mode (see Figure S4), such curve crossing is not relevant, failing to render a relevant vibrational excitation, with only a few quanta being excited. However, the PECs for the doubly degenerate CCC bending/CC torsion, $v'_{24}(e_g)$, mode show some avoided crossings, although most of the excited states are strongly bound across a large range of the normal coordinate (see Figure S4). Another relevant aspect of the CCC bending/CC torsion, $v'_{24}(e_g)$, mode is the expected Jahn–Teller distortion, which results in a non-totally symmetric displacement of the potential. This is clearly noted for

the first lowest-lying excited electronic state in Figure S4 (in red). A close inspection of the figure shows a weak vibronic interaction that is in good agreement with the fine structure mainly noted in the 8.8–10.8 eV photon energy range (Figure 4).

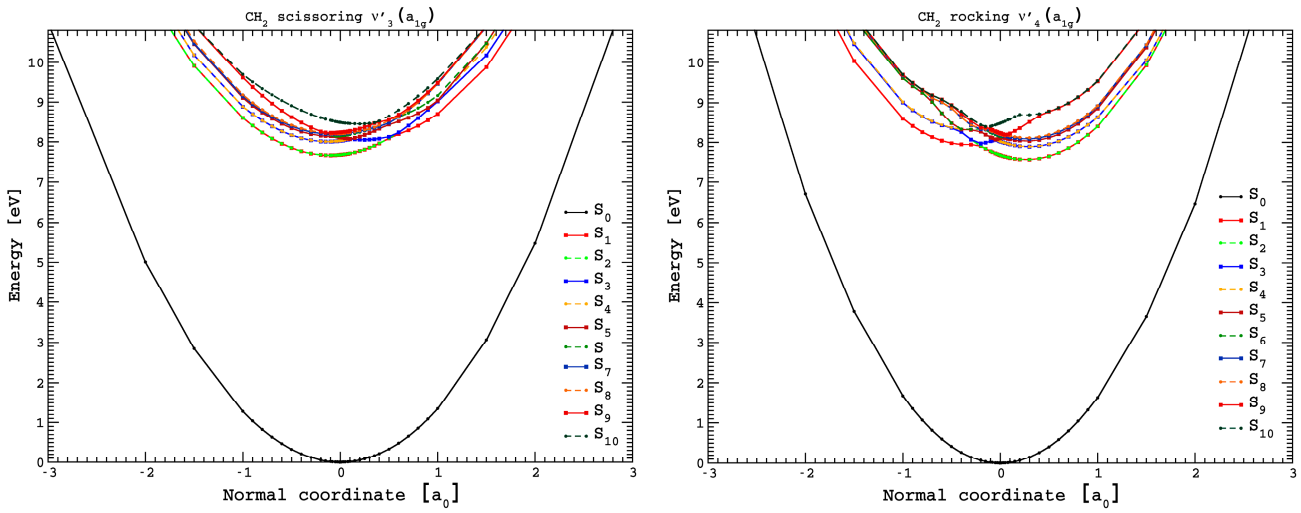

Figure 5. Potential energy curves for the ground and the ten lowest-lying singlet excited states of cyclohexane, following the CH_2 scissoring, $v_3'(a_{1g})$, and the CH_2 rocking, $v_4'(a_{1g})$, modes (in a_0 units). The calculations were performed at the TDDFT/CAMB3LYP/aug-cc-pVTZ level of theory in the C_1 symmetry group. See text for details.

The lowest-lying electronic state in Table 1, $3p\ (4a_{2u}) \leftarrow \sigma_{CC/CH}(4e_g)$, $\left(1^1E_u \leftarrow \tilde{X}^1A_{1g}\right)$, has been calculated at 8.026 eV, ~0.6 eV above the experimental value of 7.46(9) eV. The PECs in Figure 5 for CH_2 rocking, $v_4'(a_{1g})$, mode show that within the Franck–Condon region, the most probable transition occurs to the quasi-degenerate first and second electronic states at ~7.7 eV. However, if the normal coordinate is slightly reduced to +0.3 a_0, a vertical excitation energy value of the first excited electronic state in the adiabatic description occurs at 7.5 eV. This change in geometry is in agreement with the energy position of the lowest-lying absorption band (Figure 2). Another relevant aspect is related to the normal coordinate increase to −0.3 a_0, yielding a vertical excitation energy close to 8 eV. Note that at this position, the potential energy curve is rather shallow, rendering them as Rydberg in character, as obtained from the calculations. The system can now either tunnel through the almost negligible barrier (Figure 5, 3rd excited state in blue), or if the normal mode description is allowed to relax back to the equilibrium position, the excess energy may leave the molecule vibrationally (and rotationally) excited. This is in agreement with the different quanta of the CH_2 rocking, v_4' mode, being excited, as noted in the photoabsorption spectrum.

The higher energy states are mostly degenerate at the equilibrium distance, as they originate from the same ($4e_g$) and ($4a_{1g}$) molecular orbitals. The intricate molecular dynamics at these energies, and mostly visible for the CH_2 rocking, v_4' mode, are also governed by the relevant adiabatic character, mainly at the equilibrium geometry, and as the relative normal coordinate is displaced to +0.5 a_0 (Figure 5).

3.6. Absolute Photoabsorption Cross-Sections and Atmospheric Photolysis

This work reports the absolute photoabsorption cross-sections of cyclohexane in the photon energy region from 6.8 up to 10.8 eV. Table 1 lists the dominant electronic excitations and their values in units of Mb. In comparison, previous studies of the vacuum ultraviolet photoabsorption of C_6H_{12} include the wavelength regions 124–248 nm (10–5 eV) [24], 154–180 nm (8.059–6.881 eV) [25], 40–120 nm (10.332–30.996 eV) [21], and 127–182 nm

(9.733–6.819 eV) [26]. Doner et al. [24] report a cross-section value at 8.5 eV of ≈35 Mb, in good agreement with the present value of 33.96 Mb (at 8.486 eV), while Raymonda's [26] absolute value yields 16.6 Mb. Pickett et al. [25] report 1.66 Mb at 7.439 eV, a value 28% lower than the 2.28 Mb from this work, while the photoabsorption spectrum of Koizumi et al. [21] report a cross-section of ≈ 90 Mb at 10.332 eV (120 nm), slighter higher than our value of 86.28 Mb.

The radiation reaching the Earth's atmosphere, which may have an impact on a molecule's photolysis rate, occurs for wavelengths above 180 nm, and cyclohexane does not show any absorption above this value; therefore, photolysis is not a relevant process. However, gas-phase kinetics for C_6H_{12} reactions with atmospheric relevant radicals such as $^{\bullet}$OH and O_3 have been reported [1,5]. At room temperature, Harley and Cass report a reaction rate of $k_{OH} = 7.54 \times 10^{-12}$ cm^3 molec^{-1} s^{-1} [1] whereas Atkinson recommends a value of 7.21×10^{-12} cm^3 molec^{-1} s^{-1}, with an estimated overall uncertainty of ± 20% [5]. Other rate constants at 295 K are reported for gas-phase reactions with ozone, $k(O_3) \leq 1.3 \times 10^{-21}$ cm^3 molec^{-1} s^{-1}, meaning that the main atmospheric sink mechanism of cyclohexane is the reaction with the $^{\bullet}$OH radical [5,6].

4. Materials and Methods

We have performed vacuum ultraviolet (VUV) photoabsorption experiments in a wide wavelength range from 115 nm up to 182 nm (10.8–6.8 eV). The measurements were carried out using the UV1 beam line on ASTRID, Aarhus University, Denmark, and the specifics of the experiment have previously been described in detail [33,34]. Briefly, the VUV radiation passes through an absorption gas cell end station filled with a static gas sample of cyclohexane vapour at room temperature. The resolution of the photons produced by the monochromator is better than 0.08 nm [33], yielding 1, 3, and 7 meV at the low extreme, the midpoint, and the high extreme of the photon energy range scanned, respectively. The transmitted light is detected by a photomultiplier tube (PMT), and two MgF_2 transmission windows enclosing the cell set the lower wavelength limit of detection (115 nm). In each absorption scan, the sample's absolute pressure in the absorption cell is measured by a capacitance manometer (Chell CDG100D, Cambridge, UK), providing the molecular number density needed to obtain the absolute photoabsorption cross-section values, σ, in units of megabarns (1Mb $\equiv 10^{-18}$ cm^2). These are obtained from the Beer–Lambert attenuation law: $I_t = I_0 e^{(-N\sigma l)}$, where I_t is the light intensity transmitted through the gas sample, I_o is that obtained through the evacuated cell, N the molecular number density of cyclohexane, and l the absorption path length (15.5 cm). The absolute photoabsorption cross-section values were measured in the pressure range 0.02–1.34 mbar to achieve attenuations of 50% or less, hence avoiding saturation effects.

Accurate cross-section values are obtained by recording the VUV spectrum in small (5 or 10 nm) sections, allowing an overlap of at least 10 points between the adjoining sections and optimizing the pressure used for the measurement, based on the cross-sections of each section, thus allowing us to determine photoabsorption cross-sections to an accuracy of ±5%.

The liquid sample of cyclohexane (CAS number: 110-82-7) used in the VUV photoabsorption measurements was purchased from Sigma-Aldrich (St. Gallen, Switzerland), with a stated purity of ≥99.5%. The sample was degassed through repeated freeze-pump-thaw cycles before use.

Quantum chemical calculations were completed at the DFT/TDDFT [35,36] level, with a CAMB3LYP functional [37], and the aug-cc-pVTZ basis set as implemented in the GAMESS-US computational package (version GAMESS-30 Jun 2020 (R1)) [38]. Initially, the calculations were performed at the DFT level, where we optimized the geometry

of all possible conformations of cyclohexane and calculated the harmonic frequencies, verifying the stability of each conformer, as well as the total energy plus ZPE to calculate the Boltzmann distribution. Furthermore, we applied the same methodology to the cationic ground-state. For the neutral molecule, the *chair* and the *twist-boat* conformers were stable. However, the latter is 0.27 eV higher in energy than the former, and therefore, it is not expected to be relevant at room temperature (Table S1); as far as the cation is concerned, its electronic ground-state geometry is the *boat* conformation (Section 2), with bond lengths in Å and bond angles in (°), as shown in Figure S2. TDDFT calculations have been performed to compute the vertical excitation energies and oscillator strengths to aid in the assignment of the VUV absorption spectrum. In Table 1, we list the most dominant vertical excitation energies and oscillator strengths of the electronically excited states, together with the experimental values and related cross-section values. Cyclohexane belongs to the D_{3d} symmetry point group, but the calculations have been performed using the Abelian sub-group C_{2h}. In the Supplementary Table S2, a complete set of the calculated electronic transitions can be found, together with the oscillator strengths. Additionally, harmonic frequencies at the DFT-CAMB3LYP/aug-cc-pVTZ level for the neutral and the cation electronic ground-states have been calculated (Tables S3 and S4) and used to assign the major vibrational features within the mixed valence–Rydberg and Rydberg excitations in the VUV spectrum (Figures 1–4). To further our knowledge regarding the molecular structure of C_6H_{12}, we have also computed the optimized neutral and cationic ground-states, while checking all possible conformations. For the neutral molecule, the *chair* and the *twist-boat* conformers were obtained; however, the latter is 0.267 eV higher in energy than the former, and as such, it is not expected to be relevant at room temperature (Table S4); as far as the cation is concerned, its electronic ground-state geometry is the *boat* (Section 2, Figures S1 and S2).

5. Conclusions

In this joint experimental and theoretical work regarding the electronic state spectroscopy of cyclohexane, mixed valence–Rydberg and Rydberg character electronic excitations have been assigned in the energy range 6.8–10.8 eV (182–115 nm). The calculations at the DFT/CAMB3LYP/aug-cc-pVTZ level have provided vertical excitation energies and oscillator strengths for the major electronic transitions. The fine structure assignment involves vibronic excitations, with the contribution of the CH_2 scissoring, $v'_3(a_{1g})$, the CH_2 rocking, $v'_4(a_{1g})$, the C–C stretching, $v'_5(a_{1g})$, and the CCC bending/CC torsion, $v'_{24}(e_g)$, modes.

The photolysis of cyclohexane does not play a role in the Earth's atmosphere from 0 km altitude up to 50 km (the limit of the stratopause), while gas-phase kinetic studies of C_6H_{12} reactions with the $^{\bullet}$OH radical have previously been shown to be the prevalent atmospheric sink mechanism [1,5]. Time-dependent density functional theory, with the aug-cc-pVTZ basis set, has been used to calculate potential energy curves for the ten lowest-lying singlet excited states of cyclohexane along the CH_2 scissoring, $v'_3(a_{1g})$, and the CH_2 rocking, $v'_4(a_{1g})$, coordinates, mainly contributing to the spectrum yielding a relevant interchange character between Rydberg states. Other PECs have also been obtained for C–C stretching $v'_5(a_{1g})$ and CCC bending/CC torsion $v'_{24}(e_g)$ modes. The results of the rather complex nuclear dynamics involving the contribution of these modes show the need to map the potential energy surfaces and the role of possible conical intersections, which would require a computational expense that is beyond the scope of the present work.

Supplementary Materials: The following supporting information can be downloaded at: https://www.mdpi.com/article/10.3390/molecules30071493/s1, Figure S1: Electronic configuration, Cartesian coordinates, and neutral *chair* ground-state geometry of cyclohexane obtained at the DFT/CAMB3LYP/aug-cc-pVTZ level of theory. Bond lengths are in Å, and bond angles are in (°).

The plot was obtained with MacMolPlt graphical interface [39]; Figure S2: Cartesian coordinates and cationic *boat* ground-state geometry cyclohexane obtained at the DFT/CAMB3LYP/aug-cc-pVTZ level of theory. Bond lengths are in Å, and bond angles are in (°). The plot was obtained with MacMolPlt graphical interface [39]; Figure S3: Representation of a selection of cyclohexane molecular orbitals computed at the DFT/CAMB3LYP/aug-cc-pVTZ level of theory; Figure S4: Potential energy curves for the ground- and the ten lowest-lying singlet excited states of cyclohexane, following the CCC bending/CC torsion, $v'_{24}(e_g)$, and for C–C stretching, $v'_{27/28}(e_g)$, modes (in a_0 units). The calculations were performed at the TDDFT/CAMB3LYP/aug-cc-pVTZ level of theory in the C_1 symmetry group; Table S1: Total energy values with zero-point correction computed at the DFT/CAMB3LYP/aug-cc-pVTZ level of theory for cyclohexane conformers in the neutral ground-state and first excited state. Also included is the energy difference ΔE with respect to the energy of the most stable conformer; Table S2: The calculated vertical excitation energies and oscillator strengths (TD-DFT/CAMB3LYP/aug-cc-pVTZ) of *chair* cyclohexane (energies in eV). See text for details; Table S3. Harmonic frequencies computed at the DFT/CAMB3LYP/aug-cc-pVTZ level of theory for *chair* cyclohexane neutral electronic ground-state, compared with experimental data [31,40]; Table S4. Harmonic frequencies computed at the DFT/CAMB3LYP/aug-cc-pVTZ level of theory for cationic *boat-axial* ground-state cyclohexane [40].

Author Contributions: Conceptualization, E.B. and P.L.-V.; methodology, N.C.J. and S.V.H.; software, E.B., A.S.B. and M.H.F.B.; validation, M.H.F.B.; formal analysis, E.B., M.H.F.B., N.C.J., S.V.H. and P.L.-V.; investigation, N.C.J. and S.V.H.; resources, N.C.J., S.V.H. and P.L.-V.; data curation, E.B. and N.C.J.; writing—original draft preparation, E.B., M.H.F.B. and P.L.-V.; writing—review and editing, N.C.J., S.V.H., M.H.F.B. and P.L.-V.; visualization, E.B.; supervision, N.C.J., S.V.H. and P.L.-V.; project administration, S.V.H.; funding acquisition, N.C.J., S.V.H. and P.L.-V. All authors have read and agreed to the published version of the manuscript.

Funding: This research was funded by the Brazilian agencies Coordenação de Aperfeiçoamento de Pessoal de Nível Superior (CAPES), Conselho Nacional de Desenvolvimento Científico e Tecnológico (CNPq) and the European Community's Seventh Framework Program (FP7/2007-2013) under grant agreement nº 226716 (ELISA) and Fundação para a Ciência e a Tecnologia (FCT) CEFITEC (UID/00068).

Institutional Review Board Statement: Not applicable.

Informed Consent Statement: Not applicable.

Data Availability Statement: Data presented in this publication are available upon request from the authors.

Acknowledgments: E.B., A.S.B., and M.H.F.B. acknowledge the Brazilian agencies Coordenação de Aperfeiçoamento de Pessoal de Nível Superior (CAPES) and Conselho Nacional de Desenvolvimento Científico e Tecnológico (CNPq). E.B., A.S.B., and M.H.F.B. also acknowledge Carlos A. M. de Carvalho for providing computational support at LFTC-DFis-UFPR and at LCPAD-UFPR. The authors wish to acknowledge the beam time at the ISA synchrotron, Aarhus University, Denmark. P.L.-V. acknowledges his visiting professor position at Federal University of Paraná, Curitiba, Brazil.

Conflicts of Interest: The authors declare no conflicts of interest.

References

1. Harley, R.A.; Cassi, G.R. Modeling the Atmospheric Concentrations of Individual Volatile Organic Compounds. *Atmos. Environ.* **1995**, *29*, 905–922.
2. Aschmann, S.M.; Chew, A.A.; Arey, J.; Atkinson, R. Products of the Gas-Phase Reaction of OH Radicals with Cyclohexane: Reactions of the Cyclohexoxy Radical. *J. Phys. Chem. A* **1997**, *101*, 8042–8048.
3. McEnally, C.S.; Pfefferle, L.D. Experimental Study of Fuel Decomposition and Hydrocarbon Growth Processes for Cyclohexane and Related Compounds in Nonpremixed Flames. *Combust. Flame* **2004**, *136*, 155–167. [CrossRef]
4. Dahiru, U.H.; Saleem, F.; Zhang, K.; Harvey, A.P. Removal of Cyclohexane as a Toxic Pollutant from Air Using a Non-Thermal Plasma: Influence of Different Parameters. *J. Environ. Chem. Eng.* **2021**, *9*, 105023. [CrossRef]

5. Atkinson, R. Gas-Phase Tropospheric Chemistry of Volatile Organic Compounds: 1. Alkanes and Alkenes. *J. Phys. Chem. Ref. Data* **1997**, *26*, 215–290. [CrossRef]
6. Sage, A.M.; Donahue, N.M. Deconstructing Experimental Rate Constant Measurements: Obtaining Intrinsic Reaction Parameters, Kinetic Isotope Effects, and Tunneling Coefficients from Kinetic Data for OH+methane, Ethane and Cyclohexane. *J. Photochem. Photobiol. A Chem.* **2005**, *176*, 238–249. [CrossRef]
7. Chen, M.W.; Rotavera, B.; Chao, W.; Zádor, J.; Taatjes, C.A. Direct Measurement of OH and HO2 Formation in R + O2 Reactions of Cyclohexane and Tetrahydropyran. *Phys. Chem. Chem. Phys.* **2018**, *20*, 10815–10825. [CrossRef]
8. Voisin, D.; Marchal, A.; Reuillon, M.; Boettner, J.C.; Cathonnet, M. Experimental and Kinetic Modeling Study of Cyclohexane Oxidation in a JSR at High Pressure. *Combust. Sci. Technol.* **1998**, *138*, 137–158. [CrossRef]
9. Rotavera, B.; Savee, J.D.; Antonov, I.O.; Caravan, R.L.; Sheps, L.; Osborn, D.L.; Zádor, J.; Taatjes, C.A. Influence of Oxygenation in Cyclic Hydrocarbons on Chain-Termination Reactions from R + O2: Tetrahydropyran and Cyclohexane. *Proc. Combust. Inst.* **2017**, *36*, 597–606. [CrossRef]
10. Granata, S.; Faravelli, T.; Ranzi, E. A Wide Range Kinetic Modeling Study of the Pyrolysis and Combustion of Naphthenes. *Combust. Flame* **2003**, *132*, 533–544. [CrossRef]
11. Mason, N.J.; Dawes, A.; Mukerji, R.; Drage, E.A.; Vasekova, E.; Webb, S.M.; Limão-Vieira, P. Atmospheric Chemistry with Synchrotron Radiation. *J. Phys. B At. Mol. Opt. Phys.* **2005**, *38*, S893–S911. [CrossRef]
12. Serralheiro, C.; Duflot, D.; Silva, F.F.; Hoffmann, S.V.; Jones, N.C.; Mason, N.J.; Mendes, B.; Limão-Vieira, P. Toluene Valence and Rydberg Excitations as Studied by Ab Initio Calculations and Vacuum Ultraviolet (VUV) Synchrotron Radiation. *J. Phys. Chem. A* **2015**, *119*, 9059–9069. [PubMed]
13. Limão-Vieira, P.; Duflot, D.; Silva, F.F.; Lange, E.; Jones, N.C.; Hoffmann, S.V.; Ğmiałek, M.A.; Jones, D.B.; Brunger, M.J. Valence and Lowest Rydberg Electronic States of Phenol Investigated by Synchrotron Radiation and Theoretical Methods. *J. Chem. Phys.* **2016**, *145*, 034302. [CrossRef]
14. Śmiałek, M.A.; Hubin-Franskin, M.J.; Delwiche, J.; Duflot, D.; Mason, N.J.; Vrønning-Hoffmann, S.; de Souza, G.G.B.; Ferreira Rodrigues, A.M.; Rodrigues, F.N.; Limão-Vieira, P. Limonene: Electronic State Spectroscopy by High-Resolution Vacuum Ultraviolet Photoabsorption, Electron Scattering, He(I) Photoelectron Spectroscopy and Ab Initio Calculations. *Phys. Chem. Chem. Phys.* **2012**, *14*, 2056–2064. [CrossRef]
15. Martins, G.; Ferreira-Rodrigues, A.M.; Rodrigues, F.N.; de Souza, G.G.B.; Mason, N.J.; Eden, S.; Duflot, D.; Flament, J.-P.; Hoffmann, S.V.; Delwiche, J.; et al. Valence Shell Electronic Spectroscopy of Isoprene Studied by Theoretical Calculations and by Electron Scattering, Photoelectron, and Absolute Photoabsorption Measurements. *Phys. Chem. Chem. Phys.* **2009**, *11*, 11219–11231. [CrossRef]
16. Kubala, D.; Drage, E.A.; Al-Faydhi, A.M.E.; Kočíšek, J.; Papp, P.; Matejčík, V.; Mach, P.; Urban, J.; Limão-Vieira, P.; Hoffmann, S.V.; et al. Electron Impact Ionisation and UV Absorption Study of α- and β-Pinene. *Int. J. Mass Spectrom.* **2009**, *280*, 169–173. [CrossRef]
17. Limão-Vieira, P.; Eden, S.; Kendall, P.A.; Mason, N.J.; Hoffmann, S.V. VUV Photo-Absorption Cross-Section for CCl_2F_2. *Chem. Phys. Lett.* **2002**, *364*, 535–541. [CrossRef]
18. Arimura, M.; Yoshikawa, Y. Ionization Efficiency and Ionization Energy of Cyclic Compounds by Electron Impact. *Mass Spectrom.* **1984**, *32*, 375–380.
19. Holmes, J.L.; Lossing, F.P. Ionization Energies of Homologous Organic Compounds and Correlation with Molecular Size. *Org. Mass Spectrom.* **1991**, *26*, 537–541. [CrossRef]
20. Jiao, C.Q.; Adams, S.F. Electron Ionization of Selected Cyclohexanes. *J. Phys. B At. Mol. Opt. Phys.* **2011**, *44*, 17520. [CrossRef]
21. Koizumi, H.; Shinsara, K.; Hatano, Y. VUV-Optical Oscillator Strength Distributions of Molecules and Their Implications to Early Events in Radiation Chemistry. *Radiat. Phys. Chem* **1989**, *34*, 87–92.
22. Koizumi, H.; Shinsaka, I.K.; Yostu, T.; Hironaka, K.; Arai, S.; Ug, M.; Morita, M.; Nakazawa, H.; Kimura, A.; Hatano, Y.; et al. Ionization Efficiencies of C_3H_6, C_4H_8, C_6HI_2, C_2H_6O, and C_3H_8O Isomers. *Radiat. Phys. Chem.* **1988**, *32*, 111–115.
23. Shimamori, H.; Sunagawa, T. Penning Ionization and Molecular Dissociation in the Deexcitation of Neon Metastable Atoms by Some Polyatomic Molecules. *J. Phys. Chem.* **1996**, *100*, 18033–18036.
24. Doner, A.C.; Christianson, M.G.; Davis, J.C.; Koritzke, A.L.; Larsson, A.; Frandsen, K.; Rotavera, B. Vacuum-Ultraviolet Absorption Cross-Sections of Functionalized Cyclic Hydrocarbons: Six-Membered Rings. *J. Quant. Spectrosc. Radiat. Transf.* **2019**, *236*, 106603. [CrossRef]
25. Pickett, L.W.; Muntz, M.; McPherson, M.M. Vacuum Ultraviolet Absorption Spectra of Cyclic Compounds. I. Cyclohexane, Cyclohexene, Cyclopentane, Cyclopentene and Benzene. *J. Am. Chem. Soc.* **1951**, *73*, 4862–4865.
26. Raymonda, J.W. Rydberg States in Cyclic Alkanes. *J. Chem. Phys.* **1972**, *56*, 3912–3920. [CrossRef]
27. Raymonda, J.W.; Simpson, W.T. Experimental and Theoretical Study of Sigma-Bond Electronic Transitions in Alkanes. *J. Chem. Phys.* **1967**, *47*, 430–448. [CrossRef]

28. Crain, J.; Poon, W.C.-K.; Cairns-Smith, A.; Hatton, P.D. High-Pressure Raman Spectroscopic Study of Cyclohexane C_6H_{12} and C_6D_{12}. *J. Phys. Chem.* **1992**, *96*, 8168–8173.
29. Rasmussen, R.S. The Infra-Red Absorption Spectrum and Configuration of Cyclohexane. *J. Chem. Phys.* **1943**, *11*, 249–252. [CrossRef]
30. Takahashi, H.; Shimanouchi, T. Infrared Spectrum and Normal Vibrations of Cyclohexane. *J. Mol. Spectrosc.* **1964**, *13*, 43–56.
31. Shimanouchi, T. *Tables of Molecular Vibrational Frequencies*; US Government Printing Office: Washington, DC, USA, 1967; Part 1.
32. Kovac, B.; Klasinc, L. Photoelectron Spectroscopy of Adamantane and Some Adamantanones. *Croat. Chem. Acta* **1978**, *51*, 55–74.
33. Eden, S.; Limão-Vieira, P.; Hoffmann, S.V.; Mason, N.J. VUV Photoabsorption in CF_3X (X = Cl, Br, I) Fluoro-Alkanes. *Chem. Phys.* **2006**, *323*, 313–333. [CrossRef]
34. Palmer, M.H.; Ridley, T.; Hoffmann, S.V.; Jones, N.C.; Coreno, M.; De Simone, M.; Grazioli, C.; Biczysko, M.; Baiardi, A.; Limão-Vieira, P. Interpretation of the Vacuum Ultraviolet Photoabsorption Spectrum of Iodobenzene by Ab Initio Computations. *J. Chem. Phys.* **2015**, *142*, 134302. [CrossRef] [PubMed]
35. Bauernschmitt, R.; Ahlrichs, R. Treatment of Electronic Excitations within the Adiabatic Approximation of Time Dependent Density Functional Theory. *Chem. Phys. Lett.* **1996**, *256*, 454–464.
36. Casida, M.E. Time-Dependent Density-Functional Theory for Molecules and Molecular Solids. *J. Mol. Struct.-Theochem* **2009**, *914*, 3–18.
37. Yanai, T.; Tew, D.P.; Handy, N.C. A New Hybrid Exchange-Correlation Functional Using the Coulomb-Attenuating Method (CAM-B3LYP). *Chem. Phys. Lett.* **2004**, *393*, 51–57.
38. Barca, G.M.J.; Bertoni, C.; Carrington, L.; Datta, D.; De Silva, N.; Deustua, J.E.; Fedorov, D.G.; Gour, J.R.; Gunina, A.O.; Guidez, E.; et al. Recent Developments in the General Atomic and Molecular Electronic Structure System. *J. Chem. Phys.* **2020**, *152*, 154102.
39. Bode, B.M.; Gordon, M.S. MacMolPlt: A Graphical User Interface for GAMESS. *J. Mol. Graphics Mod.* **1998**, *16*, 133–138.
40. Kashinski, D.O.; Chase, G.M.; Nelson, R.G.; Di Nallo, O.E.; Scales, A.N.; Vanderley, D.L.; Byrd, E.F.C. Harmonic Vibrational Frequencies: Approximate Global Scaling Factors for TPSS, M06, and M11 Functional Families Using Several Common Basis Sets. *J. Phys. Chem. A* **2017**, *121*, 2265–2273.